Design of a Shock Tube Facility to Investigate Droplet Aerobreakup

James Leung[1], Mohana Durga Prasad[2], Shyam Menon[3]

Louisiana State University, Baton Rouge, LA, 70808

The interaction between a propagating shock wave with fuel droplets forms a fundamental process occurring in several propulsion applications. The ensuing processes including droplet aerobreakup, ignition, and combustion, are strongly influenced by the droplet-shock wave interaction. This study documents the design of a shock tube facility to study droplet-shock wave interaction under controlled conditions using non-intrusive diagnostic techniques. A shock tube capable of operating up to Mach 6 using Helium as the driver gas and air as the driven gas is designed. The various dimensions of the shock tube sections including lengths, diameters, and wall thicknesses are determined. Stress analysis using FEA is conducted to ensure a minimum factor of safety requirement. Numerical simulations are also carried out to study the breakup, vaporization, and combustion processes for iso-octane droplets. Comparisons are made to study the effect of shock Mach number on the interaction processes.

I. Introduction

Interactions between a propagating shock wave and liquid fuel droplets occur in a number of propulsion system configurations such as a rotating detonation engine (Figure 1) or rocket engines. This is a complex problem, involving a number of coupled phenomena such as high-speed flow, atomization and mixing of liquid fuel, turbulent combustion, and heat transfer processes. It is desirable to study the fundamental interaction process between a propagating shock wave with fuel droplets without the complexities involved in propulsion systems.

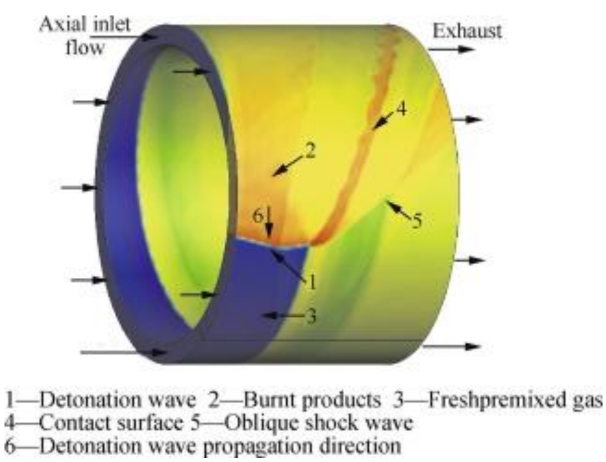

Figure 1. Flow phenomena in a rotating detonation engine [9]

[1] Graduate Research Assistant, Mechanical and Industrial Engineering Department, jleung3@lsu.edu
[2] Graduate Research Assistant, Mechanical and Industrial Engineering Department, mgurun1@lsu.edu
[3] Assistant Professor, Mechanical and Industrial Engineering Department, smenon@lsu.edu

Several previous researchers have investigated droplet-shock wave interaction phenomena using experimental approaches involving a shock tube. Pierce et al. [7], reviewed the effects of droplet-shock wave interaction with droplets larger than 100 μm and used this experiment to developed a correlation to predict ignition delay of the fuel droplet as a function of the incident shock wave strength. Kauffman et al.[4] studied the interaction of a shock wave with diethylcylohexane (DECH) and *n*-hexadecane droplets. Results such the image shown in Fig. 2 were obtained using streak photography. Shattering of the fuel droplets and their subsequent ignition was observed. Through comparisons with similar tests using water droplets, an increase in breakup time for the water droplet over the fuel droplet was observed. Droplet breakup time was also correlated to dynamic pressure.

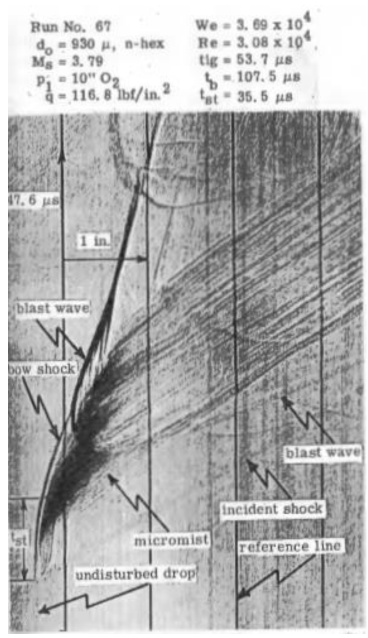

Figure 2. Streak photograph of an *n*-hexadecane droplet during interaction with a shock wave [4]

The overall goals of this project are to expand on previous efforts and address gaps in understanding with regard to the fundamental interaction processes between a liquid droplet with a shock wave. Specifically, it is desired to consider the interaction process as it applies to high Mach number shock waves (M>3) interacting with fuel droplets generally less than 100 μm in size. Previous measurements by Pierce et al. [7] and Kauffman et al. [4] were limited to relatively larger droplets of the order of 900 μm or larger in diameter. Smaller droplets, less than 100 μm in size, are more representative of droplet sizes found in sprays used in practical applications. Further, very little to no information is available for extremely small droplets at sizes on the order of 10 μm. It has been theorized that an explosive regime can exist for droplets smaller than 10 μm in size without any experimental proof and this is desired to be explored in this work. Finally, the results of this work can be used to develop regime diagrams such as the one shown in Fig. 3, which is generated for an *n*-heptane droplet undergoing combustion under quiescent conditions. A similar regime diagram developed using observations for droplets undergoing shock wave interaction can be used to correlate ignition modes of the fuel droplet to various parametric variables of interest including droplet size and shock strength, which sets the temperature and pressure conditions behind the shock wave.

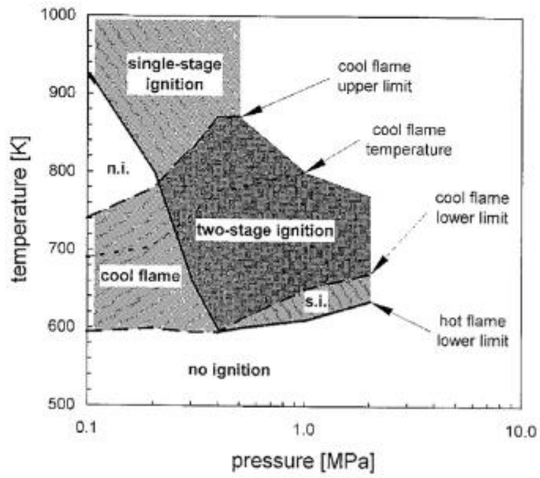

Figure 3. Ignition regime for *n*-heptane droplets [1]

The work presented in this paper focuses on the design of a shock tube facility, which will be used to achieve the overall research goals mentioned above. This work reports on the assessment of operating conditions desired to be explored in the shock tube studies. Once the appropriate operating conditions are selected, a shock tube is designed to achieve required test times at desired test conditions. The design includes the selection of lengths for the different sections of the shock tube as well as the material and wall thicknesses to safely withstand the operating pressures. Based on the design, the shock tube will be fabricated and integrated with various diagnostic techniques including high-speed imaging and laser induced fluorescence. Proposed details of the fabrication approach and diagnostics to be employed are presented. In lieu of preliminary experimental results that have been delayed due to Covid-19 related shutdown of campus research activities, simulation results considering shock wave interactions with fuel droplets under reacting and non-reacting conditions will be presented. Simulation results are analyzed and droplet breakup, vaporization, and subsequent ignition processes are discussed.

The layout of the paper is as follows. First, the experimental approach is described, including selection of operating conditions, design of the shock tube, and the proposed test procedure and diagnostic techniques. Next, the computational approach is described. Simulation results are described next, followed by conclusions and plans for future work.

II. Shock tube design and analysis

<u>Operating Conditions</u>

The goal of the shock tube is to generate shock waves up to Mach 6 in speed and study the interaction of the shock wave with liquid droplets using imaging and laser induced luminescence techniques. The Mach number requirement was established based on previous investigations of droplet-shock wave interactions. Preliminary calculations of the conditions required on the driver and driven sides to achieve the required Mach number were carried out using general pressure driven shock equations from Anderson [2]. Calculations varied the fluid composition in the driver and drive sections along with required pressures. The lower limit of pressure on the driven side was set by a vacuum pressure (2.5” Hg) that could be reliably established in a reasonable amount of time. Table 1 summarizes the conditions studied in this work. Based on the calculations, Helium is selected as the driver gas and air or oxygen as the driven gas. This would allow the required shock Mach number to be achieved with reasonable driver side pressure and an oxidizing atmosphere in the driven section permitting fuel droplet ignition to take place.

Table 1. Evaluation of shock tube operating conditions

Species		**Pressure**		**Post-shock conditions**	
Driver	Driven	Driver	Driven	Pressure	Temperature
Air	Air	7.6e10	0.008	0.3	2392
Helium	Air	19.7	0.008	0.3	2392
Helium	Oxygen	14.3	0.008	0.3	2382
		MPa		MPa	K

Shock tube design

A key consideration with respect to the shock tube design was to maximize the test time during which the droplet-shock wave interaction would be observed. This period of time corresponds to the time between the initial shock wave passing over the droplet and before any other disturbances such as the reflected shock wave or the contact surface reached the same location. It was observed that a key limitation was the shock reflection off the end wall which would limit the available test time before the reflected shock reached back at the test location. An additional consideration is the reflection of generated waves off the top and bottom walls of the shock tube. One-dimensional time-dependent calculations were carried out using a code developed at the University of Wisconsin [8]. Figure 4 shows the results from one of these calculations. Contour plots of pressure are plotted on an x-t diagram for a case that uses Helium as the driver gas and air as the driven gas with conditions chosen to give a shock Mach number of 6. Trajectories of the shock wave, contact surface, and reflected shock are shown in Fig. 4 as well as the expansion fan. The test time for this case is limited by the arrival of the reflected shock and the contact surface at the test location. The available test time is found to be about 0.5 ms (500 μs).

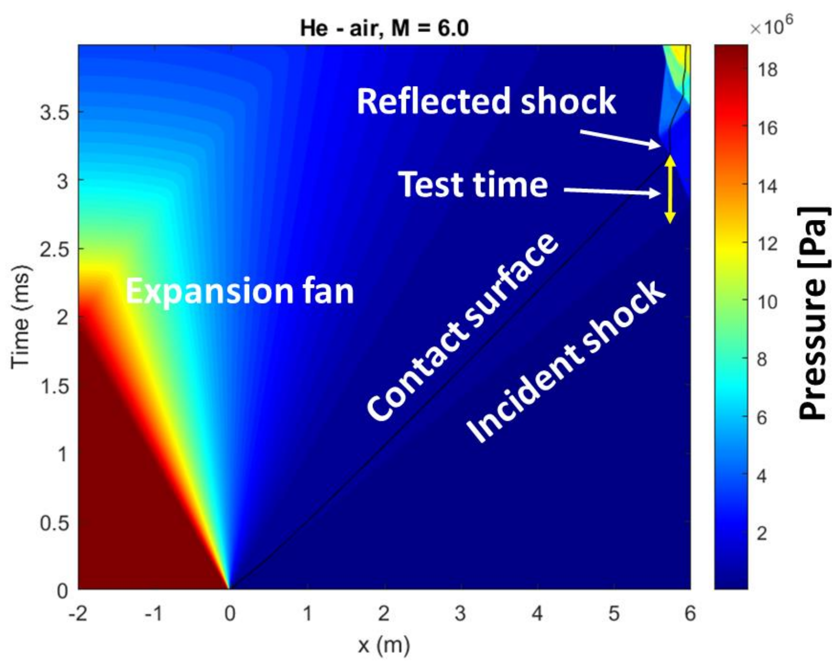

Figure 4. x-t diagram showing pressure contours for a Mach 6 Helium-Air driven shock tube.

The calculations were conducted by varying lengths of the driver and driven sections as well as a test section placed at the end of the driven section. With varying lengths of the different sections of the shock tube, simulations were conducted at different Mach numbers and the duration of test time that could be obtained with each case was calculated. The test location was established at the location in the shock tube at which the longest test duration could be obtained at the highest desired shock Mach number of 6. Then, calculations were conducted to estimate the test time duration that could be obtained at the same test location with varying shock Mach numbers. Figure 5 shows the variation of available test time as a function of shock Mach number for a case with a 2 m long driver, 6 m long driven, and 1 m long test section. The injector/test location was fixed to be at a distance of 5.7 m from the diaphragm. These dimensions were chosen for the design based on the 1-D calculations, review of shock tube designs from other research labs, as well as considerations for installation space requirements in the laboratory.

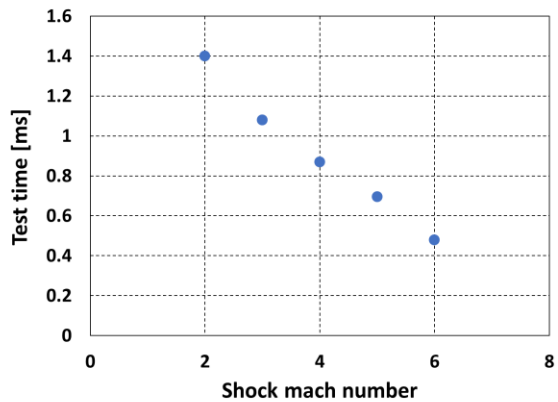

Figure 5. Variation of available test time as a function of shock Mach number for a 2 m long driver, 6 m long driven, and 1 m long test section.

1-D calculations were also used to verify the post-shock properties such as temperature and velocity as obtained from the analytical expressions. Post-shock temperature values were further used to evaluate ignition delay times for varying fuel-air mixtures. This assumes that the fuel droplet undergoes breakup, vaporization, and mixing with air to form a reactive mixture. Zero-dimensional ignition delay calculations were carried out at the post-shock pressure and temperature conditions for three fuels (*iso*-octane, *n*-heptane, and *n*-dodecane) at different equivalence ratios (0.7 and 1.2) for fuel mixtures with air and oxygen using Chemkin. Calculations were carried out for different shock Mach numbers. The goal was to estimate the ignition delay time and compare it with the test time constraints set by the design and operating conditions of the shock tube. Results of the Chemkin calculations are shown in Fig. 6. As shown by the results presented in Fig. 6, given the maximum test time available in the designed shock tube, fuel-lean and fuel-rich conditions can be studied for all three fuels for shock Mach numbers 4-6. For a shock Mach number of 3, the ignition delay is considerably longer than the test duration available in the shock tube.

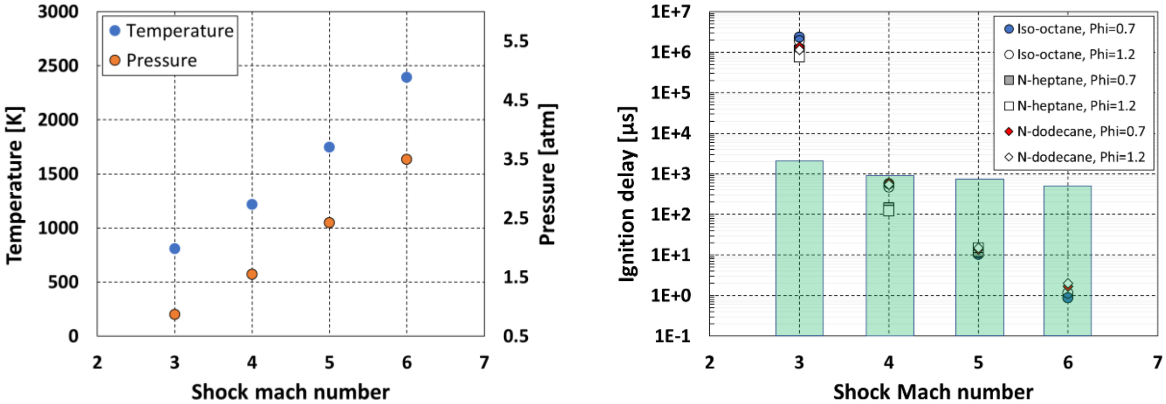

Figure 6. Post-shock temperature & pressure as a function of shock Mach number (*Left*); Ignition delay as a function of shock Mach number with bars indicating maximum test time (*Right*).

A major design consideration is to achieve the required operating conditions in the shock tube in a safe and repeatable manner. To accomplish this, shock tube is designed as a pressure vessel capable of handling the gas pressures and induced stresses with an adequate factor of safety (FOS). The driver side of the shock tube is designed to hold a peak pressure of 20 MPa corresponding to the highest operating shock Mach number of 6. The driven side experiences a lower pressure and is designed to handle up to 12 MPa. To reduce complexity, and fabricate the shock tube from components purchased off the shelf, the driver and driven sections are designed as round segments. This allows the use of commercially available pipe sections (Schedule 120) to be used for the driver and driven segments. Further, flanges for standard pipe sizes are also available off-the-shelf and can be purchased and modified as necessary for the construction of the shock tube. The test section is designed as a square section. This is primarily to aid mounting of windows needed for imaging and laser diagnostics. Table 2 summarizes the major dimensions of the shock tube segments.

Table 2. Shock tube section dimensions.

	Driver	**Driven**	**Test**
Length (m)	2	5	1
Inner diameter/dimension (in.)	4.56	4.56	3 x 3
Wall thickness (in.)	0.5	0.5	0.75
Material	SS304	SS304	SS304

Figure 7 shows an assembly drawing of the shock tube. Raised face weld-neck flanges (Schedule 120, Class 1500) are selected for their ability to form a strong seal and bond with the pipe sections through the butt-welded connections. Blank flanges are used to seal off the shock tube on either end. Test section flanges will be also of the raised face weld-neck variety but will be custom machined to enable welding to the test section which has a smaller internal cross-sectional area as compared to the driven section of the shock tube. The test section flange adapting the driven section to the test section will have an internal cross section that provides a smooth area change from a round 4.56" c/s on the driven side to the 3"x3" square c/s on the test section side. Figure 8 shows drawings of each flange type. A breech loader style is adapted for the diaphragm holder [Petersen]. The design consists of custom modifications on the flanges at the driver-driven section interface that allows a movable, sliding, threaded sleeve to be screwed on to a female-threaded section on the driven section flange. Gaskets will ensure face-seals at the driver-driven section interface. A diaphragm holder sub-assembly will be used to hold the diaphragm in place along with a blade insert to ensure repeatable diaphragm rupture. Figure 9 shows details of the breech loader design.

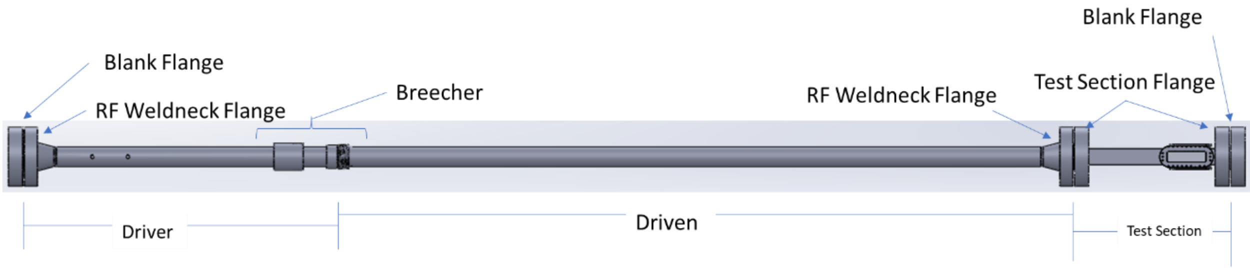

Figure 7. Shock tube assembly drawing.

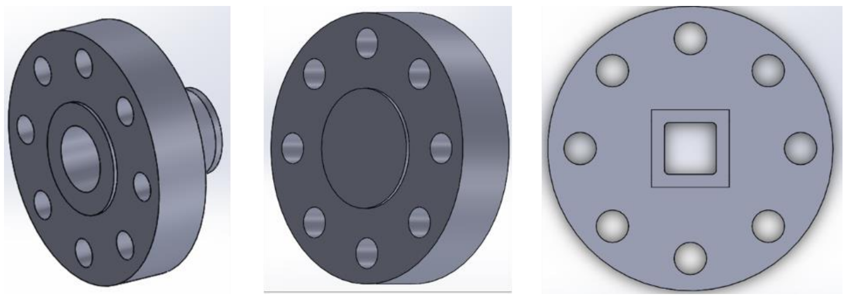

Figure 8. Raised face weld-neck flange; Blind end flange; Test section flange (*Left-Right*).

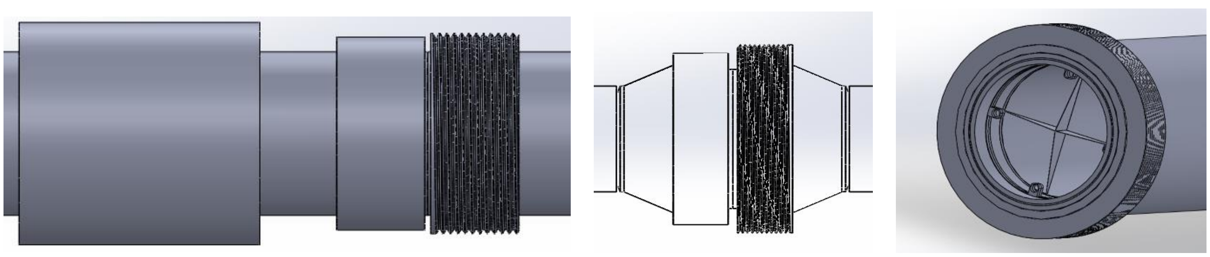

Figure 9. Breech loader design.

Figure 10 shows drawings of the test section, which as mentioned previously is designed with a square cross-section with custom flanges. The test section will be incorporated with viewing windows made of quartz/sapphire on three sides. On the fourth side, a mounting fixture will be incorporated that will allow fuel injectors or droplet generators to be installed to introduce liquid droplets into the shock tube. The windows are designed to be sandwiched between holding plates along with gaskets in such a way as to have the inner surface flush with the test section chamber.

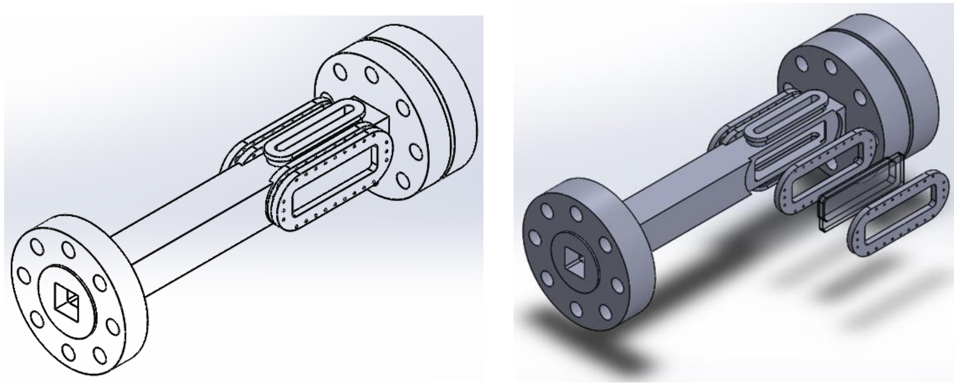

Figure 10. Test section

Figure 11 shows results of a finite element analysis done on the round driver and the square test section using the peak operating pressures for each case. The factor of safety distribution is plotted in the figures. As seen in Fig. 11, a minimum factor of safety of 7 and 2 are obtained for the driver and test sections at the peak operating pressure conditions. The values were also verified by hand calculations using hoop stress calculation.

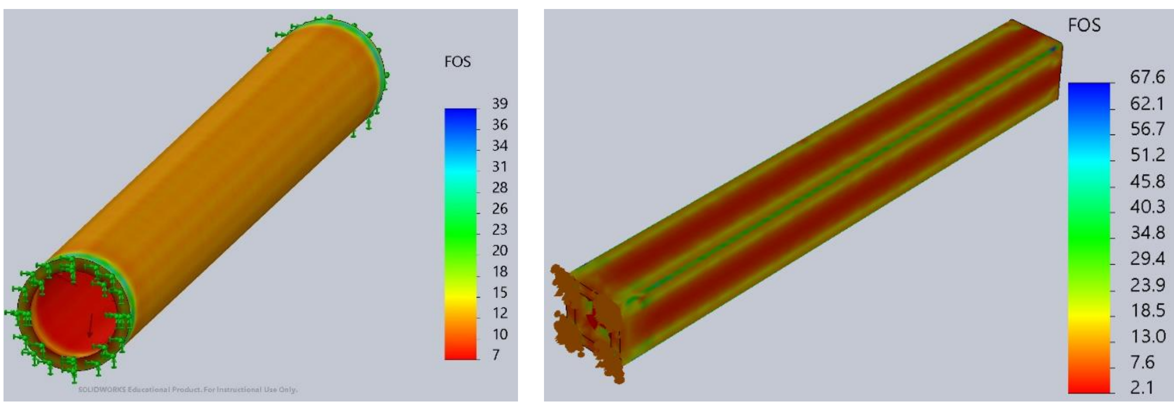

Figure 11. Stress analysis of shock tube segments showing factor of safety distribution.

Figure 12 shows an overall layout of the shock tube experiment. The shock tube will be supported on custom-fabricated floor-mounted stands. The ends of the shock tube will have additional support to account for the axial forces. The driver section will be mounted on a sliding rail mechanism to allow sufficient easy motion to replace diaphragms between shock tube tests. Compressed gas cylinders along with a vacuum pump will be used to set the needed gas composition and pressure in the driver and driven sections of the shock tube. High dynamic range Kistler pressure transducers will be used to measure pressure change and estimate shock speed and strength. Welded compression fittings will be used to connect the gas lines to the shock tube sections. A solenoid-controlled and pressure-driven spray injector will enable the spray of liquids into the test section. The current strategy for setting the shock wave in motion is to slowly fill the driver section until the rupture pressure of the diaphragm is reached.

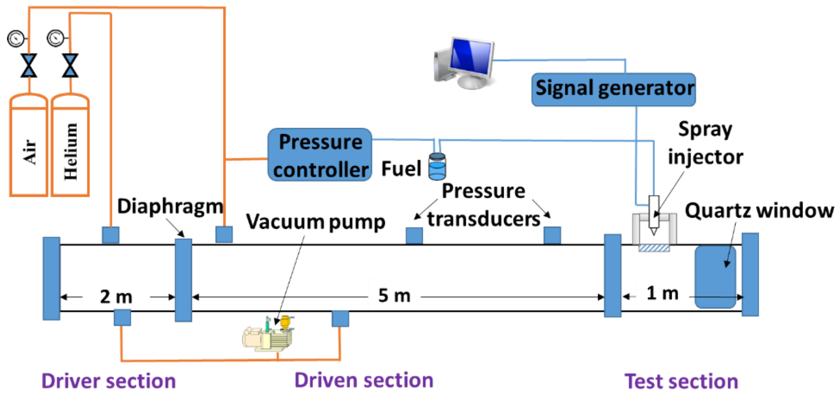

Figure 12. Layout of the shock tube facility.

Shock tube construction

As of now, the pipes and flanges for the driver and driven sections have been purchased and arrived at the machine shop on campus at LSU. Due to the extended Covid-19 related shutdown of campus activities, the progress of shock tube fabrication has been delayed significantly. Machining and setup of the shock tube experiment is now projected to be completed by the end of 2020.

Diagnostics

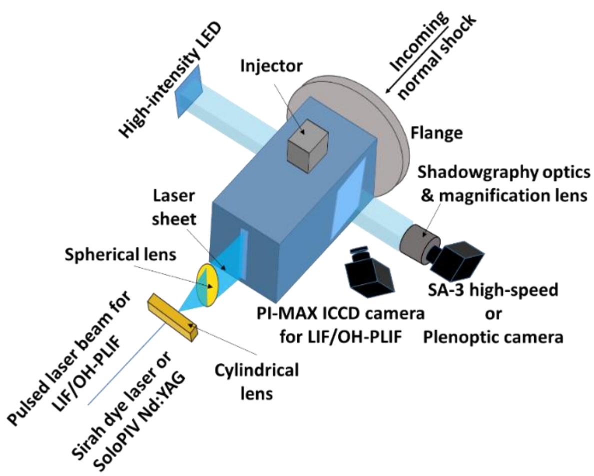

Figure 13. Test section diagnostics.

Pressure transducers mounted along the length of the driven section will be used to measure pressure and estimate shock wave speed and strength. Figure 13 shows the diagnostics proposed to be used to track droplet breakup and subsequent ignition or combustion processes in the test section. High-speed Schlieren will be pursued using a fast-pulsing LED light source of adequate wattage and a Photron SA-3 high-speed camera. A Princeton Instruments PI-MAX ICCD camera with a UVi intensifier will be used for laser induced fluorescence (LIF/PLIF) imaging in conjunction with a pulsed laser sheet generated by a PLIF dye-laser.

III. Simulation Approach

Numerical simulations to capture the transient processes involved in the shock wave induced droplet aerobreakup and subsequent ignition processes was carried out using Ansys Fluent software. The following sections describe the salient features of the numerical simulation.

- **Simulation domain and mesh**: Figure 14 shows the simulation domain along with the boundary conditions. It consists of a simple rectangular domain with assumed planar symmetry. The simulation domain represents a small section at the end of the proposed experimental shock tube, wherein the fuel droplets would be injected. The constant pressure boundary is justified, based on observations from the results of the 1-D simulation, where the pressure following the shock wave is constant for some duration of time. Since the total run time of the simulation is 4 μs, the constant pressure region would span a larger length in comparison to the streamwise dimension of the current domain. For temperature, total temperature is specified at the inlet. The primary interest is in considering the events following the passage of the shock wave over the droplet prior to any reflections off the end wall of the shock tube. Wall boundary conditions are applied to the top and right boundaries. However, all viscous effects at the walls are neglected by setting the shear input to zero. A Cartesian mesh is used in the domain which is uniformly sized in the region of interest and becomes significantly coarser outside of it, in order to reduce the computational requirements. A 100 μm droplet is located at the centerline at a distance of 500 μm from the inlet. The domain is completely filled with air and a circular drop of 100 μm diameter is patched in with properties of the desired fluid. Simulations have been performed with droplets of water and *iso*-octane.

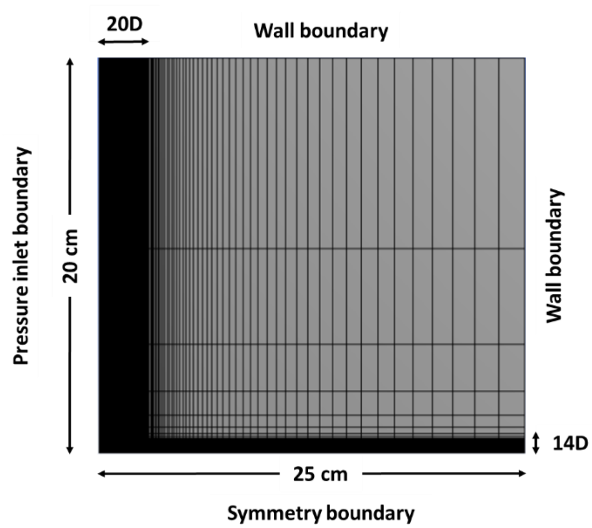

Figure 14. Physical domain and mesh used in the numerical simulations.

- **Numerical models:** The models to simulate the various physical processes are described below.
    - **Multiphase modeling:** A volume-of-fluid (VoF) model is used to simulate the droplet and gas phases. The model uses air (compressible ideal gas) and the liquid phase (water or *iso*-octane) as the two phases. Phase interactions are included for surface tension with a constant value of surface tension.
    - **Vaporization model:** A vaporization model is used that relies on the algorithm given in the work of Mohana et. al [4].

- ○ **Reaction chemistry:** A one-step reaction rate model for *iso*-octane/air mixtures is used. The Arrhenius Law used activation energy for this case is 2.587E9 J/mole and the pre-exponent factor of 1.256E8.
- ○ **Turbulence model:** A shear-stress transport (SST) k-ω model is used with turbulence damping and standard values for the various model parameters.

- **Initial conditions:** The simulation is initialized with the pressure corresponding to the driven section for the required shock Mach number, ambient temperature, and zero velocity. Liquid properties are patched into the droplet region. The gauge pressure is at 1 atm.
- **Solution methods:** Second order schemes are used for the spatial discretization. A PISO-based pressure-velocity coupling is employed. A first order implicit time stepping scheme is used.

IV. Computational Results

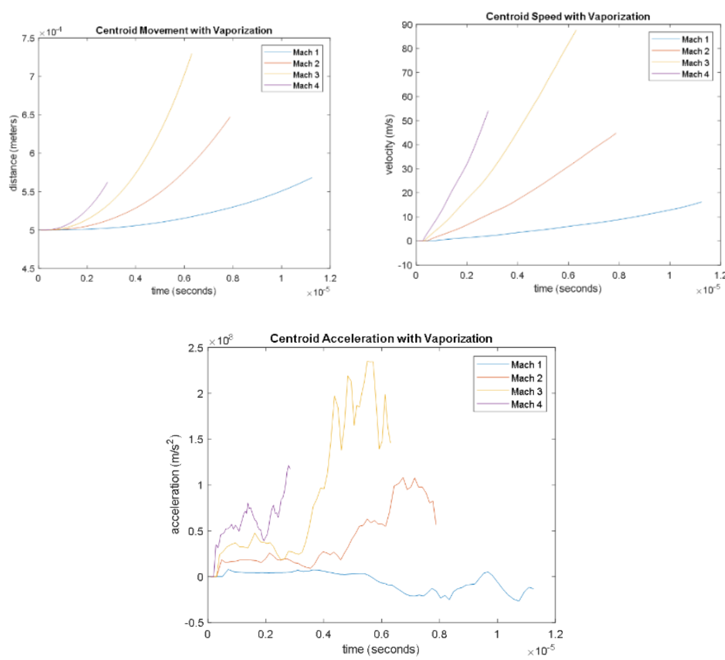

Figure 15. Iso-octane droplet centroid movement, speed, and acceleration for different shock Mach numbers.

Figure 15 shows results tracking the motion, speed, and acceleration of the centroid of a iso-octane droplet when impacted by shocks with different Mach numbers ranging from Mach 1-4. Highest acceleration is seen for the highest Mach number case as expected due to the proportionately high induced velocity that will be generated behind the shock wave. Acceleration appears to increase rapidly followed by an oscillating behavior. However, velocity appears to increase smoothly for all cases with the fastest rate for the highest Mach number as expected. Consistent results are seen with the droplet centroid position. These results are in a sense a validation case for the simulation since, similar profiles for water droplets are observed in the work by Meng [10].

Next, simulation results for three key cases will be presented and analyzed. The three cases correspond to:

- **Case A**: 100 μm *iso*-octane droplet with incident shock wave at Mach 2
- **Case B**: 100 μm *iso*-octane droplet with incident shock wave at Mach 4

- **Case C**: 100 μm water droplet with incident shock wave at Mach X

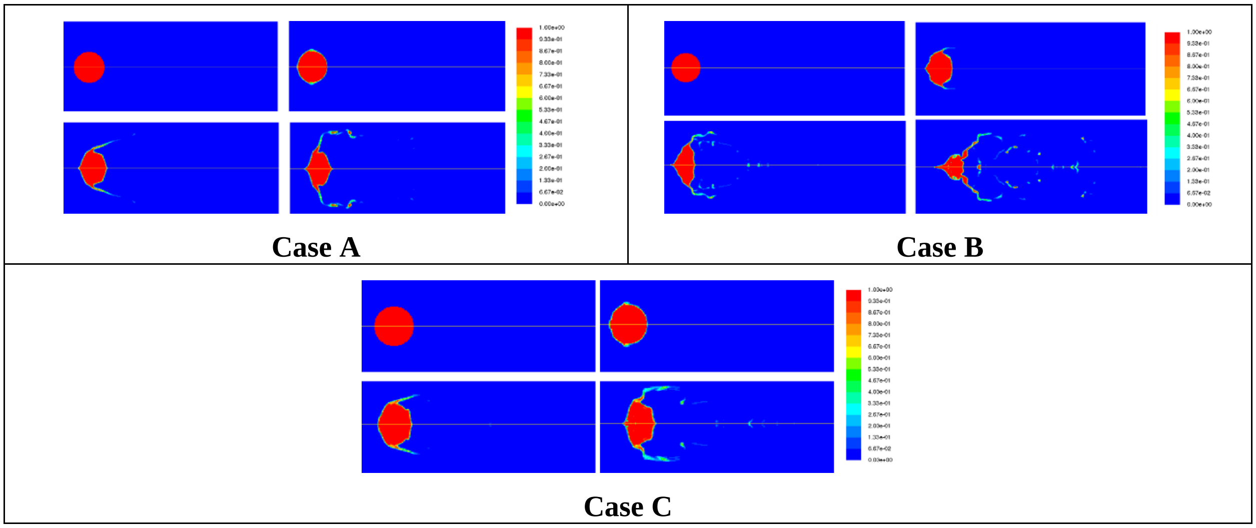

Figure 15. Volume fractions for Cases A, B, and C at different time instances (*time sequence is left to right, and top to bottom*).

Figure 15 shows isocontours of volume fractions of the liquid droplets for cases A, B, and C. For each case, contour plots are shown for four different time instances. Of the four time instances, for which results are shown in Fig. 15-17, the first time instant corresponds to before the shock wave reaches the droplet and the other three correspond to time instances after the shock wave has moved past the droplet. Considering the contour plots for liquid volume fraction in Fig. 15, the breakup of the droplet can be clearly seen. The iso-octane droplets show a distinct “spear-shaped” profile after the passing of the shock wave, which is markedly different from the flattening observed at the leading edge for the water droplet. The “spear-shape” is much more distinct for case B with the higher shock Mach number. This can likely be attributed to the higher dynamic pressure associated with the higher shock Mach number resulting in higher strain on the droplet surface. Further, the flattening of the water droplet is likely due to the higher viscosity of water (2x) as compared that of *iso*-octane. *Iso*-octane also has almost two times the vapor pressure of water at room temperature. For all three cases, a clear breakup pattern is observed with the deformation at the leading edge accompanied by the formation and breakup of ligaments from the sides of the leading edge. For case B with a higher Mach number, the ligaments appear to be stretched farther and a higher degree of droplet breakup is observed for the same time duration.

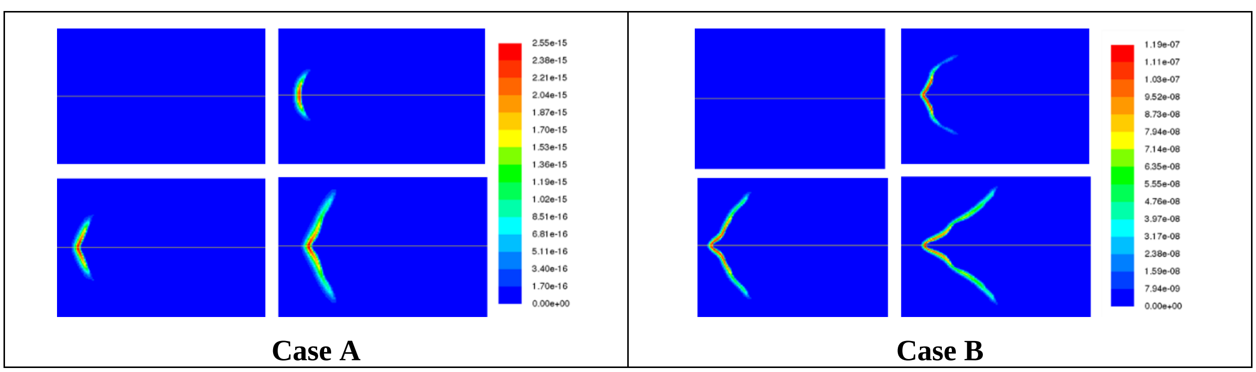

Figure 16. Reaction rates for Cases A and B (*time sequence is left to right, and top to bottom*).

Figure 16 shows the time sequence of images with the contours of reaction rate for cases A and B. Positive reaction rates are observed upon the passing of the shock wave over the iso-octane droplet. The reaction rates indicating fuel oxidation are localized along the length of the ligaments torn off the leading edges of the droplet. The highest reaction rate is observed at the very leading edge of the droplet, likely coinciding with a stagnation region formed at that location. The reaction rate decreases as one moves farther downstream along the length of the ligament. As expected, for case B, with the higher Mach number, a more extended and thinner region of positive reaction rate is observed due to the increased strain applied by the higher Mach number flow. Figure 16 can be further analyzed in conjunction with Fig. 17, which shows contour plots for vapor mass fraction of *iso*-octane for cases A and B. Distinct wake profiles of the fuel vapor are observed in the contour plots shown in Fig. 17. Significantly higher vaporization of the droplet is observed for case B with the higher shock Mach number. The fluid dynamics behind the shock wave cause the fuel vapor to be pushed towards the center line and convected downstream along with the induced flow. Comparing the contour plots of Fig. 16 and Fig. 17, combustion activity is not seen in all the regions with the vaporized fuel mass fraction as seen in Fig. 17. Positive reaction rates are not seen in the wake region immediately downstream of the droplet despite the presence of fuel vapor. This is likely due to a rich fuel-air mixture ration in the wake region due to vapor accumulation preventing ignition of the mixture.

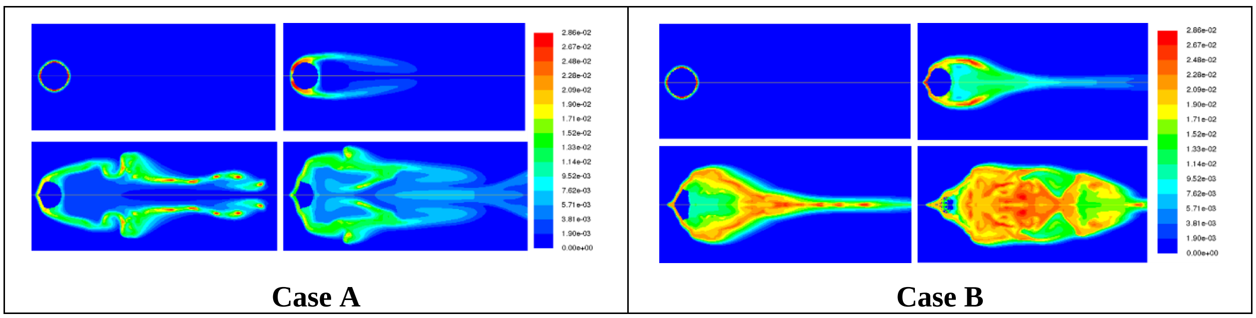

Figure 17. *Iso*-octane vapor mass fraction for Cases A and B
(*time sequence is left to right, and top to bottom*).

V.Conclusions

The interaction process between a shock wave and liquid fuel droplets forms a fundamental process, which plays a key role in several propulsion applications. This work is motivated by a desire to study the underlying physical processes involved in the interaction between a shock wave with a liquid fuel droplet. Specifically, the interest is in considering droplet sizes less than 100 microns in diameter. The approach used in this work is to design and build a shock tube experiment and subsequently evaluate the breakup process and the ensuing ignition and combustion processes using non-intrusive diagnostic techniques. Computational modeling of the interaction processes is also pursued complementary to the experimental efforts.

The present phase of this work reports on the design of the shock tube apparatus that will be used in this work. Desired operating conditions are analyzed and calculations used to arrive at gas pressure and compositions to be used in the driver and driven sections of the shock tube. Achievable test times are computed using one-dimensional codes and compared to ignition delay times to ensure testing capabilities. The driver, driven, and test sections are designed and dimensioned, and details of these are presented. Stress analysis is performed on the sections to ensure sufficient factor of safety at the operational limits of the shock tube. The proposed layout of the experiment is described along with diagnostics to be implemented.

Numerical simulations of the interaction process between a normal shock wave with single droplets of iso-octane and water are studied at conditions of varying shock Mach number. Contour plots of liquid volume fraction, reaction rate, and vapor mass fraction are studied and droplet breakup, combustion, and vaporization processes are analyzed. Shock Mach number and liquid physical properties are seen to be key drivers determining droplet breakup, vaporization, and combustion in the case of fuel droplets. The fluid dynamics driven by the induced flow behind the shock wave play a key role in the mixing phenomena affecting combustion processes in the wake of the droplet.

VI. References

[1] Aggarwal, S. K. (2014). Single droplet ignition: Theoretical analyses and experimental findings. Progress in Energy and Combustion Science, 45, 79–107

[2] Anderson, J. D. (2021). Modern compressible flow: with historical perspective. Boston: McGraw-Hill Education..

[3] Austin, J. M., & Bodony, D. J. (2011). Wave propagation in gaseous small-scale channel flows. Shock Waves, 21(6), 547–55.

[4] Gurunadhan, Mohana Durga Prasad, et al. “Numerical Simulation of Combustion in a Hybrid Rocket with Liquefying Fuels.” AIAA Propulsion and Energy 2019 Forum, 16 Aug. 2019, doi:10.2514/6.2019-4415.

[5] Kauffman, C. W., Nicholls, J. A., & Olzmann, K. A. (1971). The Interaction of an Incident Shock Wave with Liquid Fuel Drops. Combustion Science and Technology, 3(4), 165–178

[6] Marks, B., Chowdhury, A., Petersen, E. L., & Mannan, M. S. (2015). A New Facility for Studying Shock-Wave Passage Over Dust Layers. 29th International Symposium on Shock Waves 2, 1523–1528.

[7] Pierce, T., Kauffman, C., & Nicholls, J. (1975). Mechanism of ignition in shock wave interactions with reactive liquid droplets. 13th Aerospace Sciences Meeting

[8] WiSTL Wisconsin Shock Tube Laboratory. (n.d.). Retrieved from http://silver.neep.wisc.edu/~shock/tools/gdcalc.html

[9] Zhou, R., Wu, D., & Wang, J. (2015). Progress of continuously rotating detonation engines. Chinese Journal of Aeronautics, Vol 29, 15-29

[10] Meng, J. C. C. (2016). Numerical simulations of droplet aerobreakup (Doctoral dissertation, California Institute of Technology).